Single-domain near-infrared protein provides a scaffold for antigen-dependent fluorescent nanobodies

Supplemental Information

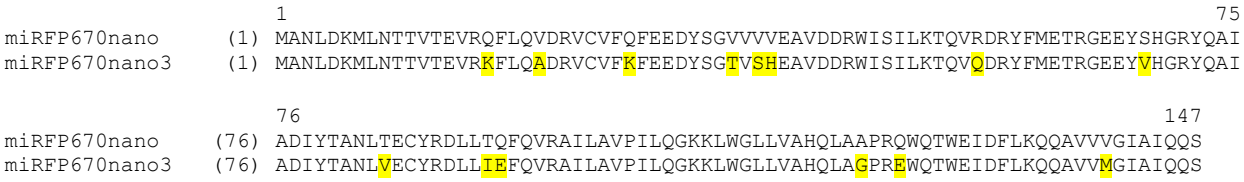

Supplementary Figure 1. Alignment of the amino acid sequences of miRFP670nano and miRFP670nano3. Mutations found in miRFP670nano3 are highlighted in yellow.

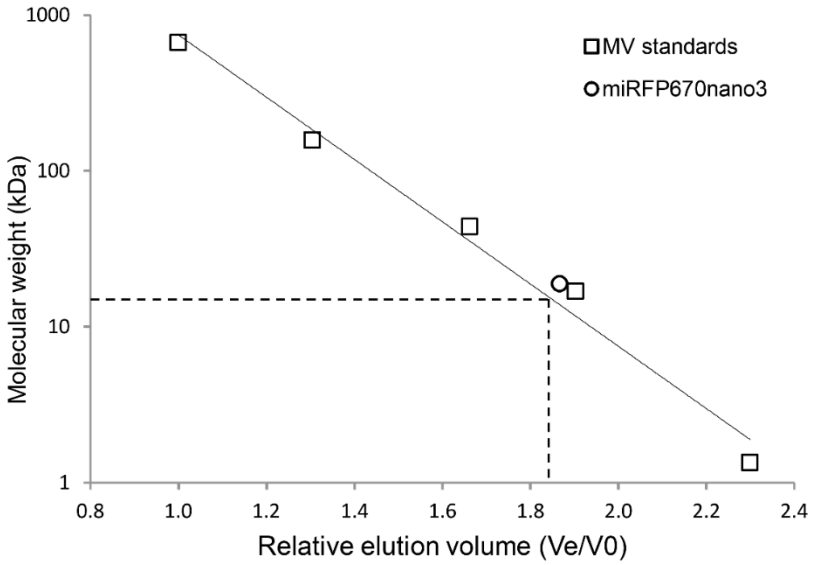

Supplementary Figure 2. Calibration plot of miRFP670nano3 size exclusion chromatography. Ve, elution volume; Vo, void volume of column.

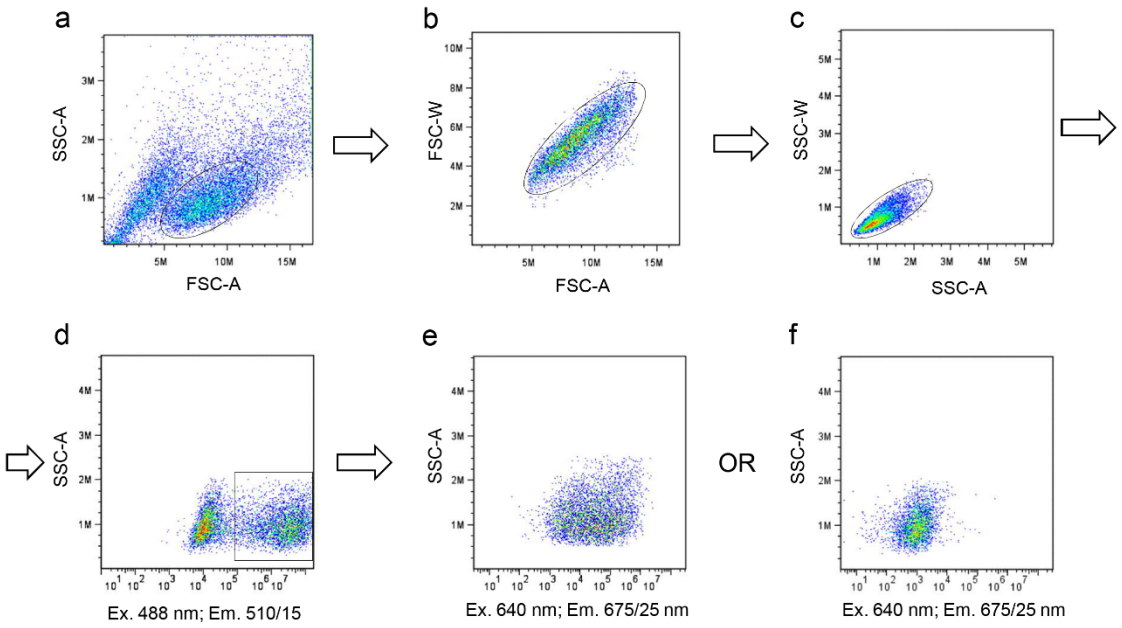

Supplementary Figure 3. Exemplifying gating strategy of flow cytometry analysis. Gating was performed using three gates, for (**a**) intact cells, (**b**) single cells, and (**c**) live cells. These cells were then gated against non-transfected cells in green (Ex. 488 nm, Em. 510/15 nm) channel for selecting EGFP positive cells (**d**). The latter cells were used to access the brightness in green and/or near-infrared (Ex. 640 nm, Em. 675/25 nm) channels (**e**, **f**).

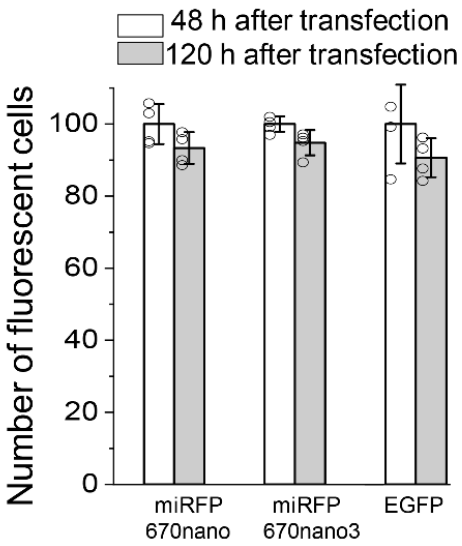

Supplementary Figure 4. Stability of miRFP670nano3 in HeLa cells. The number of FP expressing (fluorescent) HeLa cells transiently transfected with parental miRFP670nano, miRFP670nano3 or EGFP was calculated 48 h and 120 h after transfection. Gating was performed as shown in Supplementary Fig. 3. The values were normalized to the number of cells observed 48 h after transfection. Data are presented as mean values ± s.d. for $n = 4$ transfection experiments.

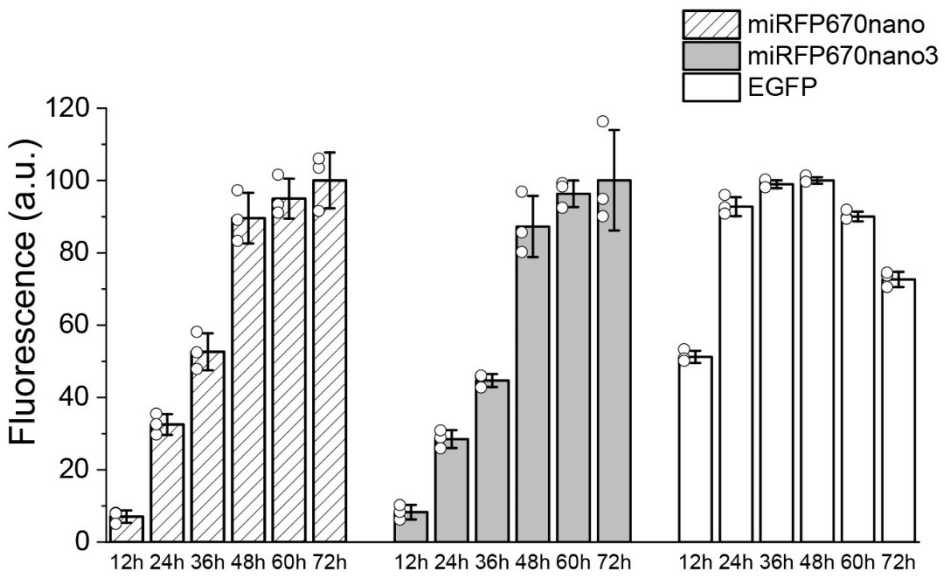

Supplementary Figure 5. Fluorescence intensity of HeLa cells transiently transfected with miRFP670nano3, miRFP670nano and EGFP measured at indicated time points after transfection. Data are presented as mean values ± s.d. for $n = 3$ transfection experiments. Fluorescence intensity was analyzed by flow cytometry using a 640 nm excitation laser and a 675/25 nm emission filter for miRFP670nano and miRFP670nano3, and a 488 nm excitation laser and a 510/15 nm emission filter for EGFP. Gating was performed as shown in Supplementary Fig. 3.

a

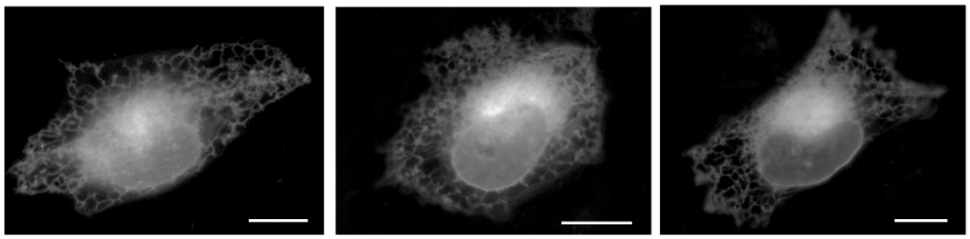

b

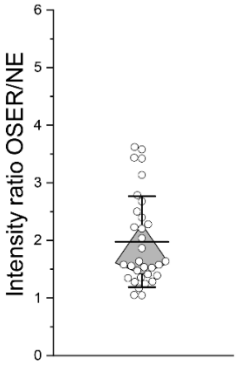

c

# of cells	% normal looking cells	# measured OSER	Ratio OSER/NE Mean fluorescence intensity±SE
250	87	32	1.98±0.14

Supplementary Figure 6. OSER assay of U-2 OS cells transfected with plasmids encoding CytERM-miRFP670nano3 fusion. (a) U-2 OS cells expressing a fusion of CytERM and miRFP670nano3. Representative images of four experiments are shown. Scale bars, 10 μm. **(b)** The ratio of the mean OSER intensity to the mean nuclear envelope intensity (NE). Each dot represents an OSER structure. Data are presented as mean values ± s.d. for $n = 32$ cells. **(c)** The results of the OSER assay. "Normal looking cells" are cells without OSER structures and incorrect localization. The 605/30 excitation and 667/30 nm emission filters were used.

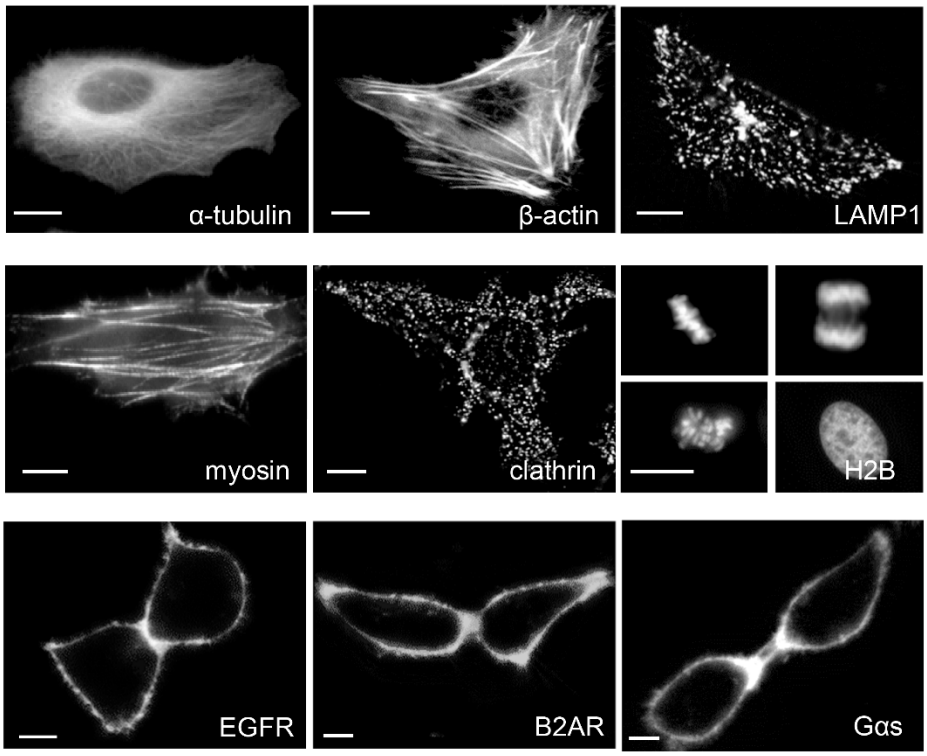

Supplementary Figure 7. Protein fusions of miRFPnano3 imaged using epifluorescence microscopy. The N-terminal fusions are α-tubulin, β-actin, myosin and vesicular protein clathrin. The C-terminal fusions are lysosomal membrane glycoprotein LAMP1, histone H2B and EGFR. The internally inserted fusions are β2 adrenergic receptor (B2AR) and G-protein α subunit (Gαs). Scale bars, 10 μm. Representative images of two experiments are shown. The 605/30 excitation and 667/30 nm emission filters were used.

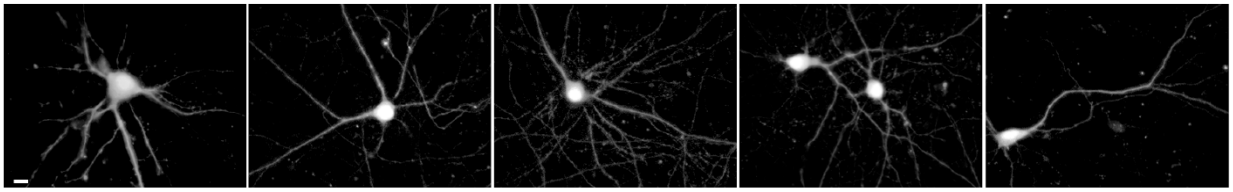

Supplementary Figure 8. Dissociated rat cortical neurons transfected with miRFP670nano3. Scale bar, 10 μm. Representative images of two experiments are shown. The 605/30 excitation and 667/30 nm emission filters were used.

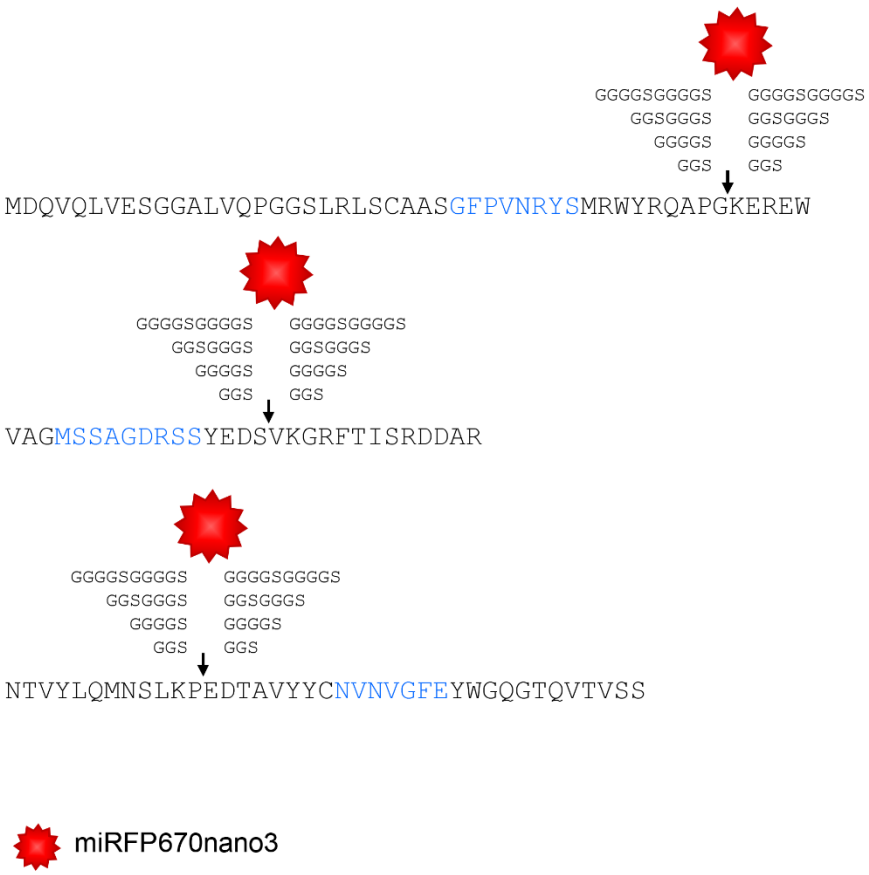

Supplementary Figure 9. The amino acid sequence of nanobody to GFP with positions for insertion of miRFP670nano3 and corresponding linkers indicated by arrows. The complementarity determining regions (CDRs) are in blue.

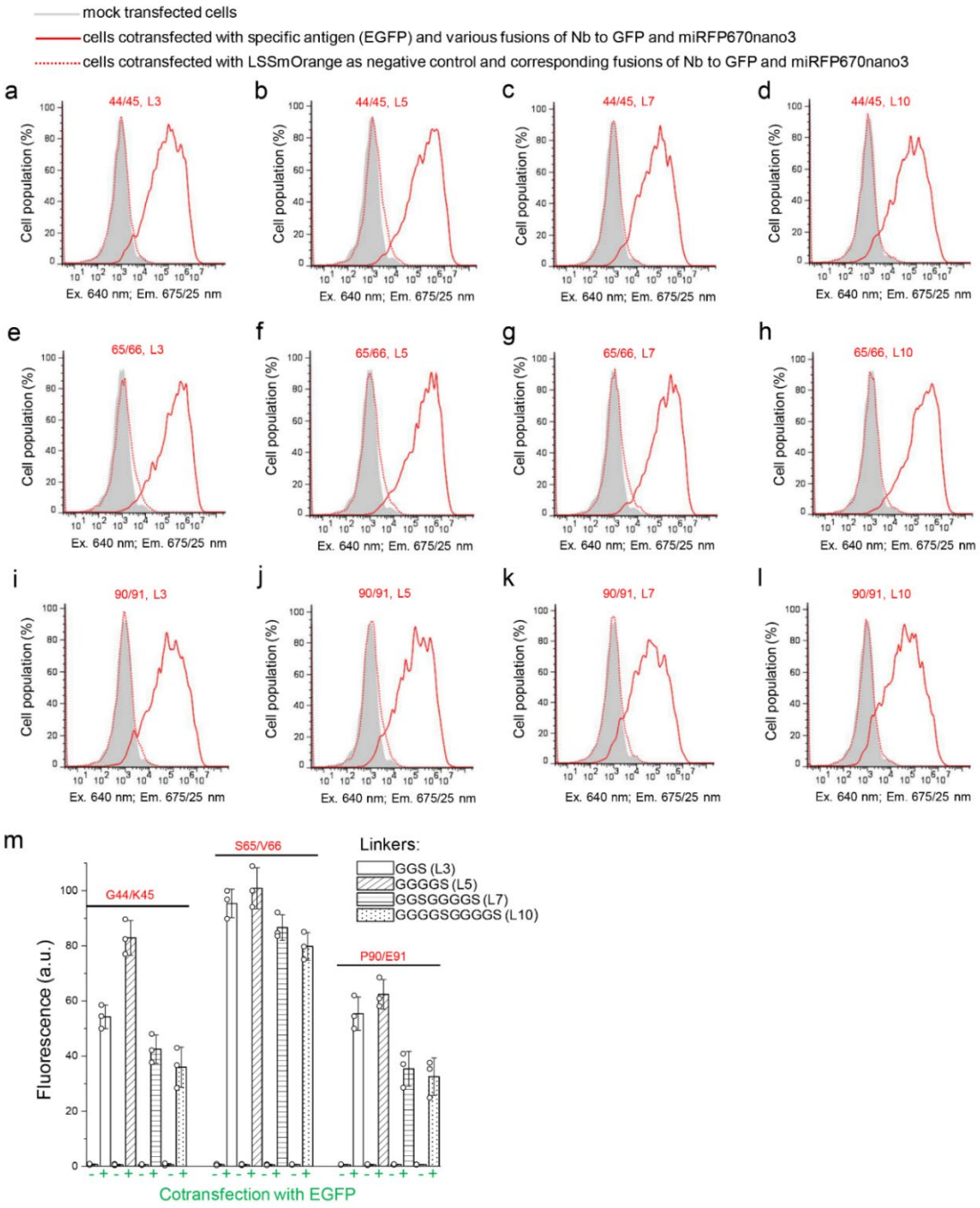

Supplementary Figure 10. Design and evaluation of NIR-Fbs. (a-l) The fluorescence intensity distribution of live HeLa cells transiently transfected with Nb_{GFP} containing miRFP670nano3 inserted at G44/K45, S65/V66 or P90/E91 sites with corresponding linkers co-expressed with or without EGFP has been analyzed using flow cytometry. Gating was performed as shown in Supplementary Fig. 3. (**m**) Quantification of the data presented in (a-l). Data are presented as mean values ± s.d. for $n = 3$ transfection experiments.

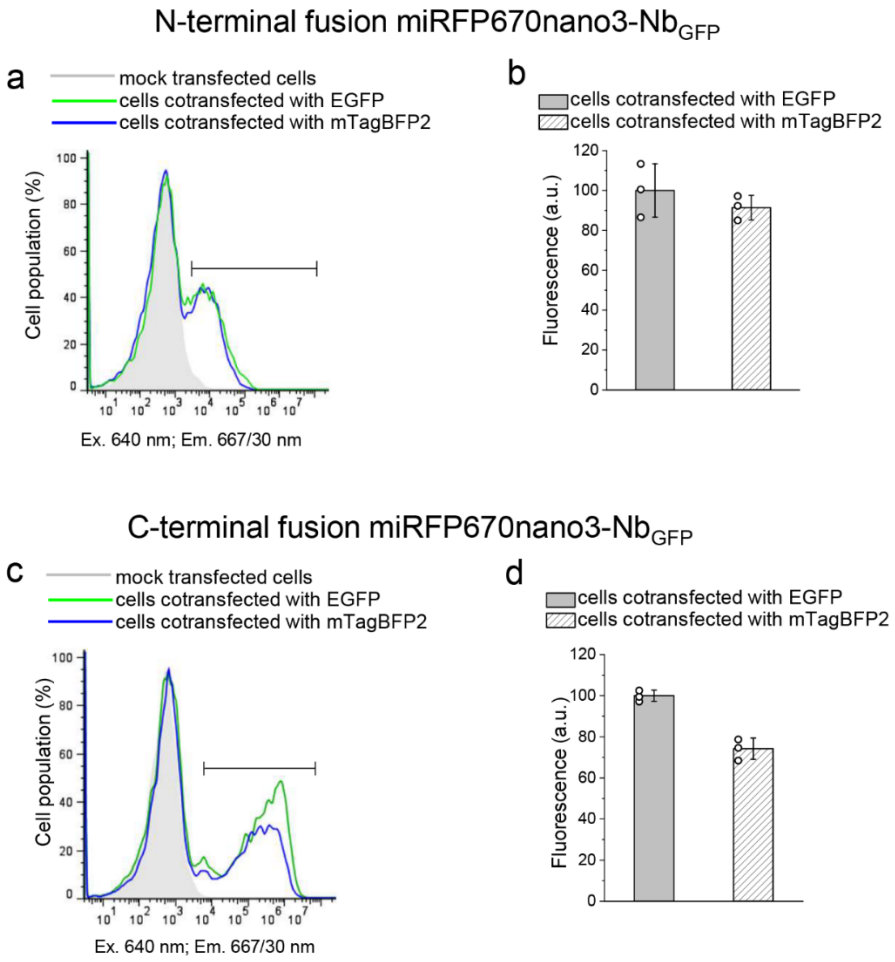

Supplementary Figure 11. Fluorescence intensity of HeLa cells transfected with Nb$_{GFP}$ N-terminally or C-terminally tagged with miRFP670nano3. (**a**) The fluorescence intensity distribution of the cells expressing N-terminal fusion miRFP670nano3-Nb$_{GFP}$ co-transfected with either cognate antigen EGFP or control antigen mTagBFP2. Gating was performed as shown in Supplementary Fig. 3. (**b**) Quantification of the data presented in (a). (**c**) The fluorescence intensity distribution of the cells expressing C-terminal fusion Nb$_{GFP}$-miRFP670nano3 co-transfected with either cognate antigen EGFP or control antigen mTagBFP2. (**d**) Quantification of the data presented in (c). In (b, d) data are presented as mean values ± s.d. for $n = 3$ transfection experiments. The miRFP670nano3 fluorescence intensity was analyzed by flow cytometry using a 640 nm excitation laser and a 667/30 nm emission filter.

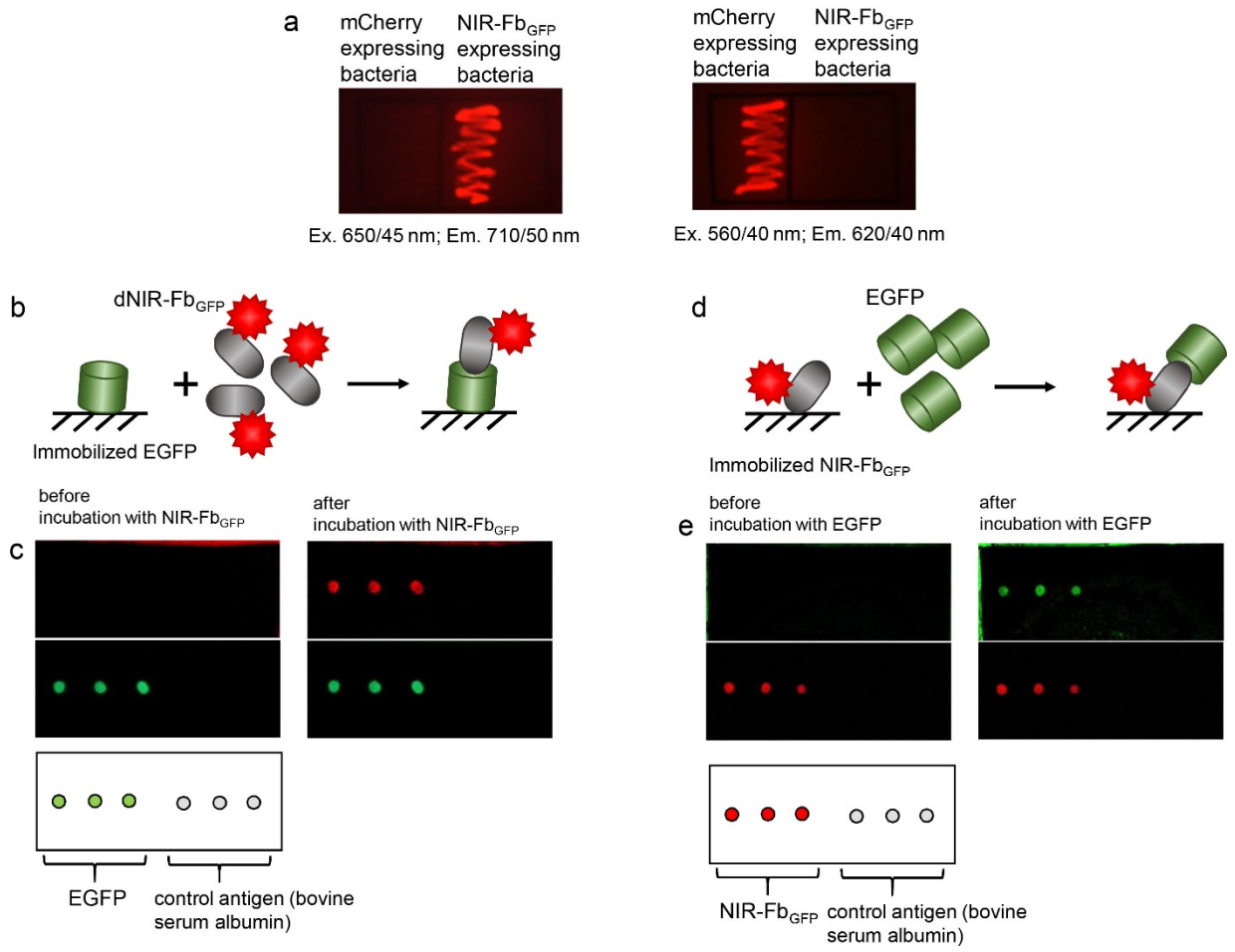

Supplementary Figure 12. Analysis of antigen-binding properties of NIR-Fb$_{GFP}$ using dot-blot assay. (a) Live *E.coli* bacterial cells expressing mCherry (negative control) and NIR-Fb$_{GFP}$. Bacterial streaks were imaged with Leica M205FA fluorescence stereomicroscope using filter sets ex. 650/45 nm and em. 710/50 nm for NIR-Fb$_{GFP}$ and ex. 560/40 nm and em. 620/40 nm for mCherry. **(b)** Schematics of the dot-blot immunoassay for detection of EGFP immobilized on nitrocellulose membrane using NIR-Fb$_{GFP}$. **(c)** Detection of immobilized EGFP using NIR-Fb$_{GFP}$. **(d)** Scheme of the dot-blot immunoassay for detection of NIR-Fb$_{GFP}$ immobilized on nitrocellulose membrane using EGFP. **(e)** Detection of immobilized NIR-Fb$_{GFP}$ using EGFP. Membranes were imaged with Leica M205FA fluorescence stereomicroscope using filter sets ex. 650/45 nm and em. 710/50 nm for NIR-Fb$_{GFP}$ and ex. 480/40 nm and em. 535/50 nm for EGFP.

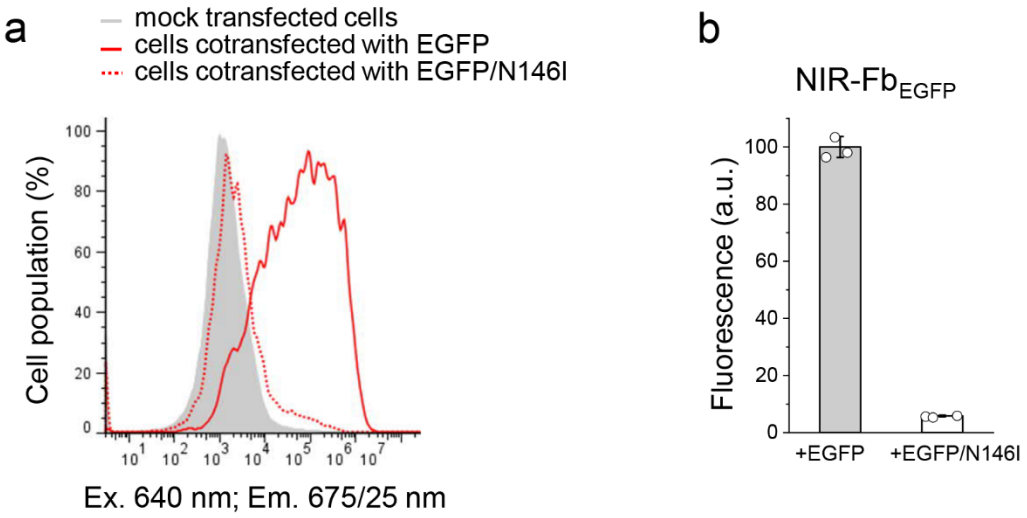

Supplementary Figure 13. Analysis of NIR-Fb specificity to an antigen. (a) The fluorescence intensity distribution of live HeLa cells transiently transfected with NIR-Fb$_{GFP}$ co-expressed with EGFP or with EGFP/N146I mutant was analyzed using flow cytometry. Gating was performed as shown in Supplementary Fig. 3. **(b)** Quantification of the data presented in (a). Data are presented as mean values ± s.d. for $n = 3$ transfection experiments.

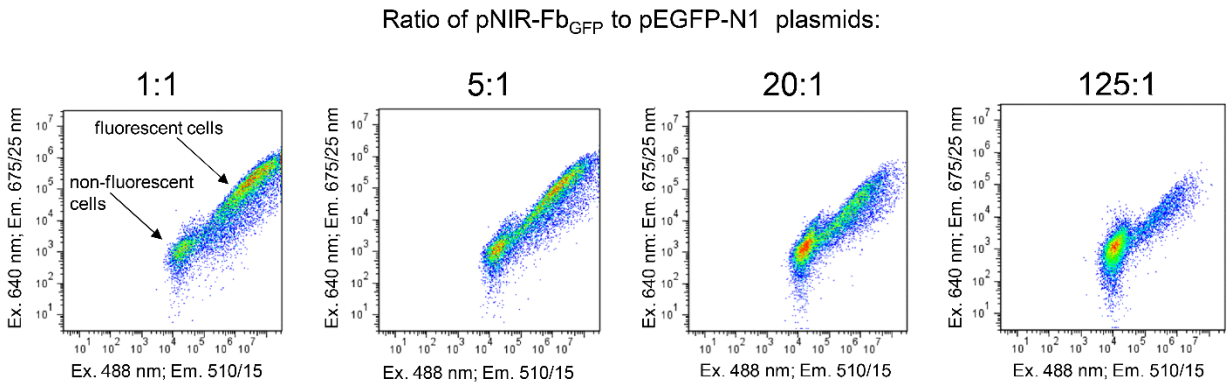

Supplementary Figure 14. Fluorescence intensity of HeLa cells transfected with the same amount of a pNIR-FbGFP plasmid and indicated ratios of a pEGFP-N1 plasmid to the pNIR-FbGFP plasmid. The fluorescence intensity was analyzed by flow cytometry using a 640 nm excitation laser and a 675/25 nm emission filter for miRFP670nano3, and a 488 nm excitation laser and a 510/15 nm emission filter for EGFP. The data are presented as the intensity dot plots of miRFP670nano3 (ordinate axis) versus EGFP (abscissa axis) fluorescence.

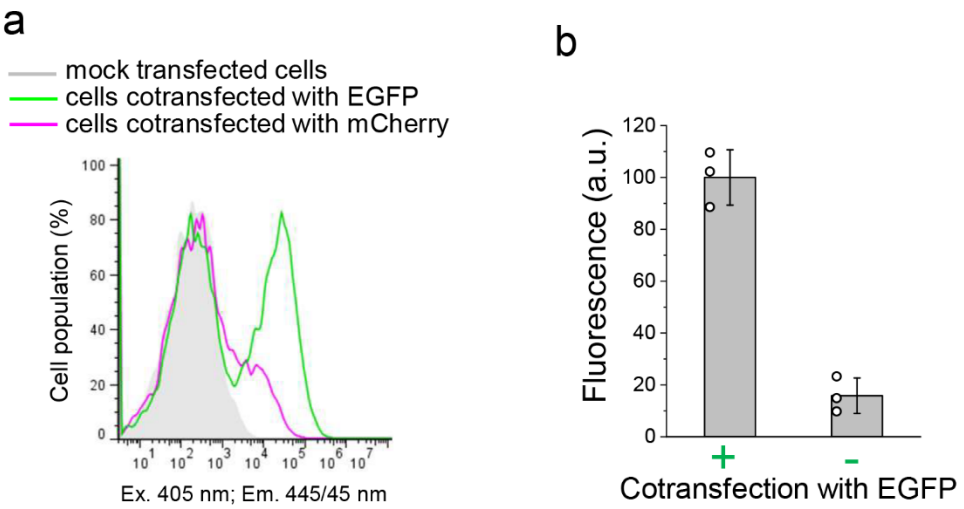

Supplementary Figure 15. NIR-Fb$_{GFP}$ fused to mTagBFP2 is stabilized by binding to antigen similarly to unfused NIR-Fb$_{GFP}$. (a) Fluorescence intensity of HeLa cells expressing NIR-Fb$_{GFP}$ fused with mTagBFP2 co-transfected with either EGFP or mCherry. Gating was performed as shown in Supplementary Fig. 3. (**b**) Quantification of the data presented in (a). Data are presented as mean values ± s.d. for $n = 3$ transfection experiments. The fluorescence intensity was analyzed using flow cytometry using a 405 excitation laser and a 445/45 emission filter. The mTagBFP2 brightness in cells co-transfected with EGFP was assumed to be 100%. Error bars, s.d. (n=3; transfection experiments).

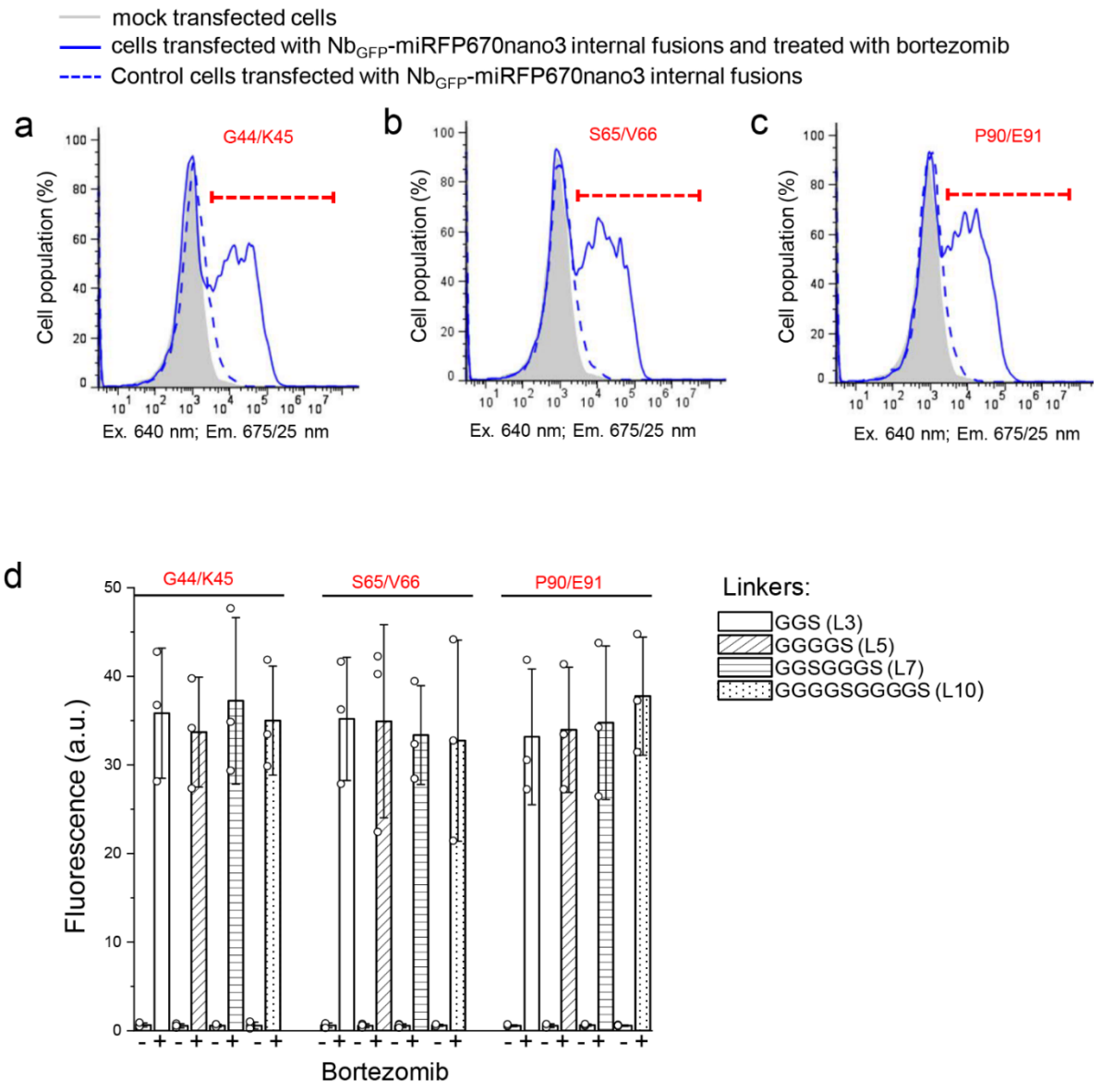

Supplementary Figure 16. NIR-Fb behavior in mammalian cells: stabilization by antigen binding and proteasomal degradation in unbound state. Mean fluorescence intensity of HeLa cells transiently transfected with Nb$_{GFP}$, containing miRFP670nano3 inserted at **(a)** G44/K45, **(b)** S65/V66 or **(c)** P90/E91 sites before and after 4 h of incubation with 10 μM proteasome inhibitor bortezomib. **(d)** Mean fluorescence intensity of HeLa cells transiently transfected with Nb$_{GFP}$ containing miRFP670nano3 inserted at the indicated sites via corresponding linkers before and after 4 h of incubation with 10 μM bortezomib. Gating was performed as shown in Supplementary Fig. 3. Data are presented as mean values ± s.d. for $n = 3$ transfection experiments.

Supplementary Figure 17. Alignment of the amino acid sequences of the Nbs to GFP, mCherry, all actins, human β-catenin, ALFA-tag peptide, dihydrofolate reductase from *E.coli*, HIV's protein antigens p24 and gp41, and Nb21 and Nbm6 to SARS-CoV-2's spike protein. The insertion position of miRFPnano3 is indicated by the arrow.

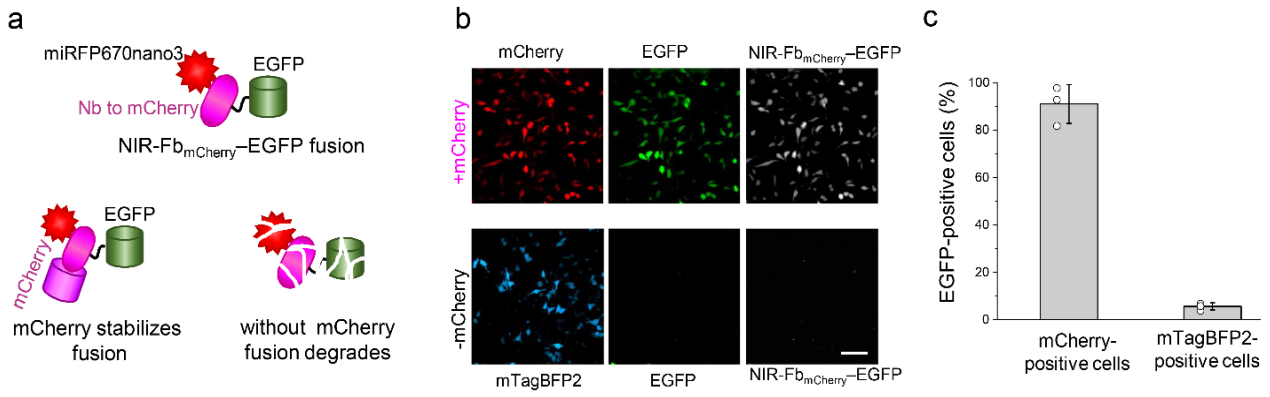

Supplementary Figure 18. Antigen-dependent stabilization of NIR-Fb fusion-partner. (a) Schematic representation of NIR-Fb$_{mCherry}$–EGFP fusion. If mCherry is not expressed by cells, the fusion degrades. (**b**) Fluorescent images of live HeLa cells transiently co-transfected with NIR-Fb$_{mCherry}$–EGFP and mCherry cognate antigen (top row), or with NIR-Fb$_{mCherry}$–EGFP and mTagBFP2 control (bottom row). Scale bar, 100 μm. Representative images of two experiments are shown. (**c**) Quantification of the data presented in (b). Data are presented as mean values ± s.d. for $n = 3$ transfection experiments. For the miRFP670nano3, EGFP and mCherry imaging, the 605/30 nm excitation and 667/30 nm emission, 485/20 excitation and 525/30 nm emission, and 560/25 nm excitation and 607/36 nm emission filters were used.

Supplementary Table 1. Properties of monomeric NIR FPs designed from various bacterial photoreceptors and red-shifted GFP-like FPs mCherry and mCardinal.

NIR FP	Ex, nm	Em, nm	Extinction coefficient, $M^{-1}cm^{-1}$	Quantum yield, %	Molecular brightness *vs.* miRFP670 nano, %	p*K*a$_1$ (acid)	p*K*a$_2$ (alkali)	Photostability in HeLa cells, $t_{1/2}$, s	Brightness in mammalian cells *vs.* miRFP670nano, % [a]	Ref.
miRFP670nano	645	670	95,000	10.8	100	3.7	9.0	545	100	[1]
miRFP670nano3	645	670	129,000	18.5	233	4.2	11	500	412	this work
miRFP670	642	670	87,400	14.0	119	4.5	9.5	183	117	[2]
miRFP703	674	703	90,900	8.6	76	4.5	>9.5	394	61	
miRFP709	683	709	78,400	5.4	41	4.5	9.2	192	42	
SNIFP	697	720	75,000 [b]	2.2	16	4.5	>9.0	n.a.	n.a.	[3]
mIFP	683	704	82,000	8.4	67	4.5	9.2	54	26	[4, 5]
BDFP1.5	688	711	74,000	5.0	36	2.0	>10	1310 [c]	0.5 [c]	[6]
mCherry	587	610	72,000	22.0	154	4.5	n.d.	68 [d]	n.d.	[7]
mCardinal	604	659	87,000	19.0	160	5.3	n.d.	730 [d]	n.d.	[8]

miRFP670nano3 is highlighted in bold.

[a] Unless otherwise stated, it is determined as NIR fluorescence in live HeLa cells 72 h after transfection with no supply of exogenous BV and after normalization to the fluorescence of co-transfected EGFP.

[b] Estimated from SNIFP absorption spectrum in Supplementary Figure 2a in original paper[3].

[c] Based on the comparison with smURFP in HEK293 cells in[6].

[d] Measured with different light sources in original papers[7, 8].

.

Supplementary Video S1. Z-stack of two-photon images showing miRFP670nano3-labeled neurons (red) in the neocortex of a 14-weeks-old anesthetized *Cx3cr1* $^{GFP/+}$ mouse with labeled microglia (white). Data were acquired with an Olympus XLUMPlanFl 20× 1.0 NA objective at 2.5× optical zoom 5 weeks after stereotactic injection of a custom AAV9-hSYN-miRFP670nano3 vector (0.4 μl at ~650 μm cortical depth). 920 nm light from a Coherent Ultra II laser was used to excite both fluorophores. The 525/70 and 645/75 emission filters were employed to collect EGFP and miRFP670nano3 fluorescence, respectively. Recording depth from the pial surface is indicated in the upper right corner. Center and left images were acquired simultaneously. Images on the right show their overlay. Scale bar, 100 μm.

Supplementary Video S2. Z-stack of two-photon images showing miRFP670nano3-labeled neurons (red) in the neocortex of a 13-weeks-old anesthetized *Cx3cr1* $^{GFP/+}$ mouse with labeled microglia (white). Data were acquired with an Olympus XLUMPlanFl 20× 1.0 NA objective at 1.7× optical zoom four weeks after stereotactic injection of a custom AAV9-hSYN-miRFP670nano3 vector (0.4 μl at ~400 μm cortical depth). 930 nm light from a Coherent Ultra II laser was used to excite both fluorophores. The 525/70 and 645/75 emission filters were employed to collect EGFP and miRFP670nano3 fluorescence, respectively. Recording depth from the pial surface is indicated in the upper right corner. Center and left images were acquired simultaneously. Images on the right show their overlay. Scale bar, 100 μm.

Supplementary Video S3. Z-stack of two-photon images showing miRFP670nano3-labeled neurons (red) in the lumbar spinal dorsal horn of a 12.5-weeks-old anesthetized *Cx3cr1* $^{GFP/+}$ mouse with labeled microglia (white). Data were acquired with an Olympus XLUMPlanFl 20× 1.0 NA objective at 1.0× optical zoom five weeks after stereotactic injection of a custom AAV9-hSYN-miRFP670nano3 vector (0.4 μl at ~50 μm depth). 925 nm light from a Coherent Ultra II laser was used to excite both fluorophores. The 525/70 and 645/75 emission filters were employed to collect EGFP and miRFP670nano3 fluorescence, respectively. Recording depth from the pial surface is indicated in the upper right corner. Center and left images were acquired simultaneously. Images on the right show their overlay. Scale bar, 100 μm.

References

1. Oliinyk, O.S., Shemetov, A.A., Pletnev, S., Shcherbakova, D.M. & Verkhusha, V.V. Smallest near-infrared fluorescent protein evolved from cyanobacteriochrome as versatile tag for spectral multiplexing. *Nature Communications* **10** (2019).
2. Shcherbakova, D.M. et al. Bright monomeric near-infrared fluorescent proteins as tags and biosensors for multiscale imaging. *Nat Commun* **7**, 12405 (2016).
3. Kamper, M., Ta, H., Jensen, N.A., Hell, S.W. & Jakobs, S. Near-infrared STED nanoscopy with an engineered bacterial phytochrome. *Nat Commun* **9**, 4762 (2018).
4. Yu, D. et al. A naturally monomeric infrared fluorescent protein for protein labeling in vivo. *Nat Methods* **12**, 763-765 (2015).
5. Shemetov, A.A., Oliinyk, O.S. & Verkhusha, V.V. How to Increase Brightness of Near-Infrared Fluorescent Proteins in Mammalian Cells. *Cell Chem Biol* **24**, 758-766 e753 (2017).
6. Ding, W.L. et al. Small monomeric and highly stable near-infrared fluorescent markers derived from the thermophilic phycobiliprotein, ApcF2. *Biochim Biophys Acta* **1864**, 1877-1886 (2017).
7. Shaner, N.C. et al. Improved monomeric red, orange and yellow fluorescent proteins derived from Discosoma sp. red fluorescent protein. *Nat Biotechnol* **22**, 1567-1572 (2004).
8. Chu, J. et al. Non-invasive intravital imaging of cellular differentiation with a bright red-excitable fluorescent protein. *Nat Methods* **11**, 572-578 (2014).